



## OPEN ACCESS

## EDITED BY

Ya Ping Wang,  
East China Normal University, China

## REVIEWED BY

Hao Wu,  
East China Normal University, China  
Yupeng Pan,  
Hangzhou Dianzi University, China

## \*CORRESPONDENCE

Zhirui Zhu,  
✉ zhuzr2001@163.com

RECEIVED 03 November 2025

REVISED 04 January 2026

ACCEPTED 08 January 2026

PUBLISHED 06 February 2026

## CITATION

Wu Y, Zhu Z, Wu Q, Xu G and Chen G (2026)  
Experimental investigation on volumetric  
strain accumulation of saturated marine sands  
subjected to wave-induced complex cyclic  
loading.  
*Front. Earth Sci.* 14:1738337.  
doi: 10.3389/feart.2026.1738337

## COPYRIGHT

© 2026 Wu, Zhu, Wu, Xu and Chen. This is an  
open-access article distributed under the  
terms of the [Creative Commons Attribution  
License \(CC BY\)](https://creativecommons.org/licenses/by/4.0/). The use, distribution or  
reproduction in other forums is permitted,  
provided the original author(s) and the  
copyright owner(s) are credited and that the  
original publication in this journal is cited, in  
accordance with accepted academic practice.  
No use, distribution or reproduction is  
permitted which does not comply with  
these terms.

# Experimental investigation on volumetric strain accumulation of saturated marine sands subjected to wave-induced complex cyclic loading

Yanshen Wu<sup>1</sup>, Zhirui Zhu<sup>2\*</sup>, Qi Wu<sup>2</sup>, Gaofeng Xu<sup>3</sup> and Guoxin Chen<sup>2</sup>

<sup>1</sup>China Oilfield Services Ltd. (COSL Geophysical, Marine Survey and Geotech Company), Tianjin, China, <sup>2</sup>Institute of Geotechnical Engineering, Nanjing Tech University, Nanjing, China, <sup>3</sup>Zhejiang Huadong Geotechnical Investigation & Design Institute CO, Ltd., Hangzhou, China

The dilatancy of marine sands highly depends on the complex cyclic stress paths caused by waves. A series of the axial-torsional coupling cyclic loading tests are performed on the saturated marine sands under isotropically consolidated condition by using the Hollow Cyclic Apparatus (HCA). The dilatant behavior of saturated sands is investigated under complex stress paths, as well as the correspondent mathematical model. The results are summarized as follows: The volumetric strain of sands is composed of a completely reversible component and an irreversible component. The cyclic stress path has significant effects on the development of volumetric strain. The equivalent cyclic stress ratio (ESR), which is defined as the ratio of the mean value of the maximum stress in a loading cycle to the initial effective confining pressure can be used as an index to quantitatively characterize the cyclic stress paths of the soil sample under wave-induced axial-torsional loading. The accumulated volumetric strain ( $\epsilon_{vd,ir}$ ) increment may be uniquely correlated to the applied ESR, which accumulates linearly with the increase of ESR. By introducing ESR, A stress-dependent normalized  $\epsilon_{vd,ir}$  incremental model of the saturated sands under complex cyclic loading was presented. Retrospective simulation of a laboratory test using the proposed model shows good agreement, calibrating the reliability of the model. However, the modified Byrne model significantly underestimates the volumetric strain accumulation of the saturated marine sands under the axial-torsional coupling cyclic loading, which was built on the data of direct shear tests. The proposed model provides a practical tool for estimating the long-term accumulation of volumetric strain and consequent settlement in offshore foundation soils, such as those supporting wind turbines or pipelines, under the action of complex storm-wave loading.

## KEYWORDS

complex cyclic stress path, continuous rotation of the principal stress direction, cyclic stress path, dilatancy, equivalent cyclic stress ratio

## 1 Introduction

With the intensification of global marine resource exploitation, the oceans have emerged as crucial elements in international port engineering, offshore energy facilities, cross-sea corridors, and island infrastructure development (Juan et al., 2025). The foundations of these large-scale projects are exposed to long-term cyclic wave loads, and their dynamic response characteristics directly impact the long-term safety and stability of superstructures (Chen et al., 2024). Saturated marine sand, as the primary constituent of these foundations, demonstrates volumetric deformation behavior under wave loads, which is a key factor in controlling the development of cumulative deformation and settlement. The cyclic stresses induced by waves are characterized by variable amplitudes, involve the rotation of the principal stress axis, and follow complex stress paths (Yue et al., 2023). At present, the soil dynamics theory based on conventional continental sand reveals significant limitations when applied to this special geological material. For instance, conventional models derived from triaxial tests on continental sands often neglect the effects of continuous principal stress axis rotation and the coupled variation of axial and shear stresses, which are inherent to wave-induced loading. Furthermore, empirical parameters calibrated for simple stress paths (e.g., uniaxial compression) may lead to significant underestimation of volumetric strain when applied to the complex elliptical paths experienced by marine sands. Therefore, there is a substantial theoretical necessity and engineering urgency to investigate the variable characteristics of saturated marine sand under wave loads.

Ishihara and Towhata (1983) initially observed the phenomenon of continuous rotation of the principal stress axis of seabed soil induced by travelling waves. They derived the analytical solution for the alternating shear and deviatoric stresses generated by surface waves with equal-wavelength harmonics in an elastic seabed. Their findings indicated that the principal stress axis rotates continuously through 180°, while the deviatoric stresses remain invariant. Based on the analytical solution of the dynamic response of a seabed with finite thickness under the action of linear regular waves, Wang et al. (2017) demonstrated that the stress path of a finite-thickness elastic seabed under the influence of linear regular waves takes the form of a non-standard ellipse. Drawing on the analytical solution of the dynamic response of a finite-thickness seabed under the action of standing waves, Zhou et al. (2021) deduced the dynamic stress paths of soil elements within the seabed. They concluded that for a soil element located at the wave node, its dynamic stress path is a line segment on the longitudinal axis; for one located at the wave antinode, it is a line segment on the transverse axis; and for those situated between the wave node and the wave antinode, the dynamic stress path assumes a non-standard elliptical shape. These aforementioned elliptical stress paths share the characteristics of continuous rotation of the principal stress axis and continuous variation of the dynamic stress amplitude. Consequently, it is necessary to simultaneously account for the coupling effect of vertical and shear forces.

Under both drained and undrained cyclic shear conditions, the volume variations in saturated sandy soil and the response of pore-water pressure manifest an inherently consistent physical

mechanism. The volumetric strain ( $\epsilon_v$ ) generated by drained cyclic shear corresponds to the growth characteristics of the excess pore-water pressure ( $u_e$ ) induced by cyclic shear under undrained conditions, suggesting that both stem from the same physical process. Moreover, when the excess pore water pressure generated during undrained cyclic loading dissipates, the resulting soil deformation can be mainly ascribed to the compaction effect of sand under drained conditions. Experimental findings demonstrate that there is a coupling effect between the shear behavior and the volume compression response in saturated sandy soil, where cyclic shear induces plastic volumetric strain. The pore-pressure models established by Martin et al. (1975), Dobry et al. (1985), and Chen et al. (2019) all share a common premise: in strain-controlled constant amplitude cyclic tests, there is a quantitative relationship between the increment of volumetric strain produced by one cycle under drained conditions and the increment of pore pressure caused by the same strain-amplitude cycle under undrained conditions, and this ratio is a constant modulus independent of the testing method. Zhang (2000) found that the shear-induced volumetric change in sandy soils consists of reversible and irreversible volumetric strain components through consolidated drainage cycle torsional shear tests. Notably, the shear-compression coupled pore-pressure model developed by Chen et al. (2019) based on the CTD (Compressive Tensile Test) experiment significantly underestimated the cumulative strain  $\epsilon_{vr}$  in cyclic axial-torsional composite shear tests. This phenomenon indicates that both cyclic loading patterns and stress-path configurations significantly influence the cumulative strain behavior of saturated sand under cyclic loading conditions.

While the aforementioned studies provide valuable insights into soil behavior under principal stress rotation, most are conducted under idealized or simplified stress paths (e.g., pure rotation, fixed amplitude). A critical gap remains in quantitatively linking the full spectrum of elliptical stress path parameters (amplitude, shape, inclination) to the volumetric strain accumulation of marine sands under conditions that more faithfully simulate the multi-directional nature of real wave loading. A multitude of studies (Duku et al., 2008; Yee et al., 2014; Wu et al., 2020; Symes et al., 1988; Miura et al., 1986; Gutierrez et al., 1991; Yuan et al., 2024; Xiong et al., 2016) have demonstrated that the volumetric deformation characteristics during drainage shear are notably influenced by factors such as the initial effective consolidation stress, relative density, and the magnitude of cyclic shear stress. Qin et al. (2024) conducted drainage experiments with varying cyclic stress paths to systematically investigate the effects of relative density ( $D_r$ ), cyclic stress path, and stress level on strain characteristics ( $\epsilon_v$ ) in saturated coral sand bodies. The experiments demonstrated that cyclic stress paths significantly influence the accumulation rate of  $\epsilon_v$  within the stress loop, while the peak volume strain ( $\epsilon_{vp}$ ) increases in an arctangent function pattern with repeated cycles. Moreover, the experimental results indicated that pure principal stress axis rotation leads to bulk shrinkage in soil. The plastic strain increment of sand shows inconsistency between the principal stress axis and the plastic strain axis, which implies remarkable non-coaxial behavior. Tong et al. (2010) conducted pure principal stress axis cyclic rotation drainage tests, keeping the amplitude of the effective principal stress acting on the specimen constant while cyclically rotating the principal stress axis between

0° and 180°. Their research findings disclosed that pure principal axis rotation can generate plastic deformation of the same order of magnitude as that of fixed principal stress axis monotonic shear. The intermediate principal stress coefficient exerts a significant influence on the deformation characteristics of sand under this stress path. These studies offer valuable perspectives for comprehending the drainage shear behavior of marine sand under complex dynamic stress paths induced by complex wave loads.

The drainage shear characteristics of marine sandy soils, being one of their essential mechanical properties, occupy a prominent position in the theoretical framework of soil dynamics ontology (Zhang and Wang, 2024). As reviewed above, although significant progress has been made in understanding cyclic soil behavior, predictive models for volumetric strain accumulation often rely on parameters calibrated from tests with fixed principal stress directions or simple shear modes (e.g., Martin et al., 1975; Byrne, 1991; Chen et al., 2019). A robust framework that can incorporate the defining features of wave-induced stress paths—variable amplitude, principal stress rotation, and coupled axial-shear components—is still lacking for marine sands. To overcome the limitation of CSR in characterizing complex stress paths with continuous principal stress rotation, this study introduced the Equivalent Cyclic Stress Ratio (ESR), which physically represents the average intensity of cyclic shear stress experienced by a soil element over a complete loading cycle. To examine the drainage shear characteristics of marine sand under wave-induced elliptical dynamic stress paths, a series of isotropic consolidation axial-torsional coupled cyclic loading tests were carried out on saturated fine sand from the Bohai Sea using a hollow cylindrical torsion-shear apparatus (HCA). By introducing characteristic parameters that quantify both the shape and magnitude of elliptical stress paths, this research explores the dilatancy behavior of saturated marine sand under wave-induced complex stress paths and establishes a quantitative approach for assessing volumetric strain.

## 2 Test materials and methods

### 2.1 Test apparatus and specimen stress conditions

The tests employed the Hollow Cylinder Apparatus (HCA) manufactured by GDS Instruments Ltd., UK, to conduct drained coupled axial-torsional cyclic loading tests. The HCA facilitates coupled cyclic loading in both the axial and torsional directions. Axial and torsional loads are applied at the base of the specimen. Force transducers for measuring axial force and torque are located at the specimen top, while displacement transducers for measuring axial displacement and angular rotation are positioned at the specimen base. The maximum dynamic axial and torsional loads are 10 kN and 30 Nm, respectively, with a maximum loading frequency of 5 Hz for both modes. Confining pressures (outer cell pressure and inner cell pressure) and back pressure are applied and measured using standard pressure/volume controllers, with a maximum capacity of 2 MPa. Back pressure is applied at the specimen base, and pore pressure is measured at the specimen top. A detailed description of the HCA testing accuracy

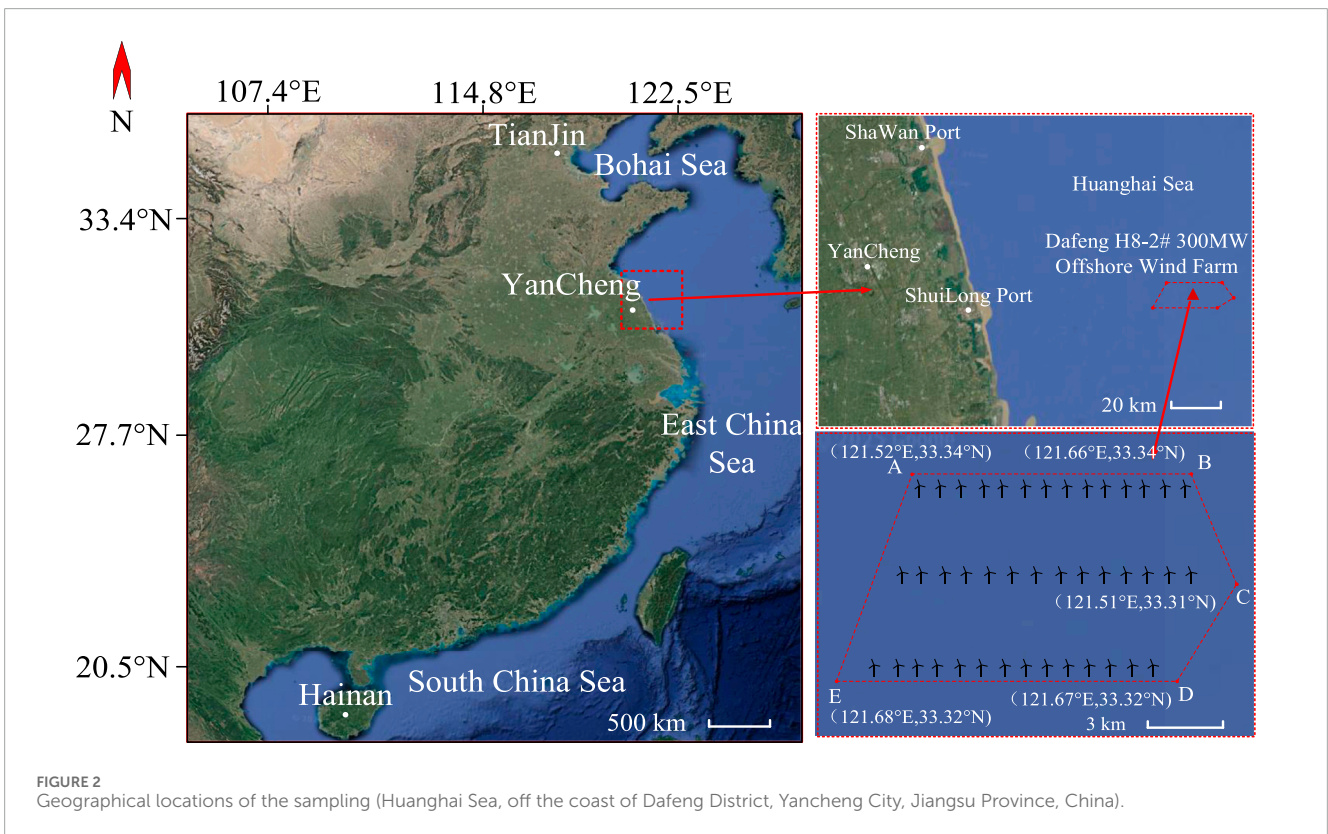
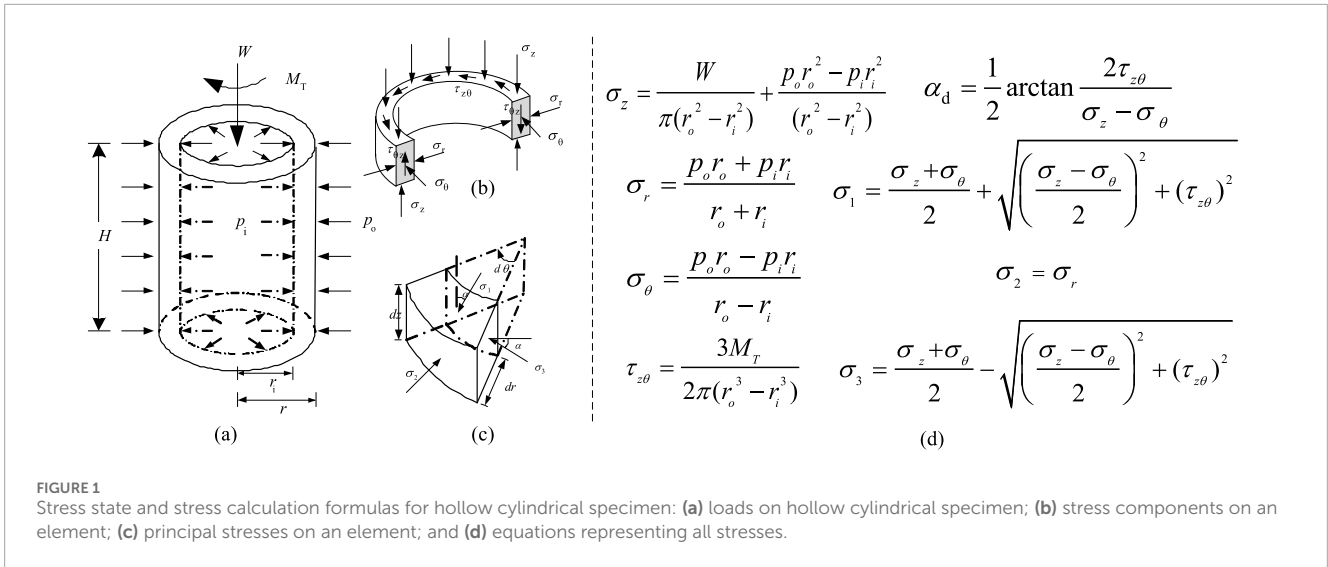
and the data processing procedures employed can be found in references (Chen et al., 2016; Zienkiewicz et al., 1980; Prasanna and Sivathayalan, 2021).

Figure 1a illustrates the stress state of a thin-walled specimen element in the HCA. The instrument's control and loading parameters indicated in the figure are as follows:  $r_i$ ,  $r_o$  = inner and outer radii of the specimen, respectively;  $u_i$ ,  $u_o$  = inner radial displacement and outer radial displacement of the specimen during shearing, respectively;  $p_i$  = inner cell pressure,  $p_o$  = outer cell pressure;  $W$  = axial force;  $M_T$  = torque. The stress components acting on the thin-walled specimen element are depicted in Figures 1b,c:  $\sigma_z$  = axial stress;  $\sigma_r$  = radial stress;  $\sigma_\theta$  = hoop (circumferential) stress;  $\tau_{z\theta}$  = shear stress in the plane perpendicular to the radial direction;  $\sigma_1$ ,  $\sigma_2$ ,  $\sigma_3$  = major, intermediate, and minor principal stresses of the element, respectively;  $\alpha$  = orientation angle of the major principal stress;  $\theta$  = torsional displacement (angle of twist) generated in the specimen during shearing. The relationships between these stress components are presented in Figure 1d.

### 2.2 Test materials, preparation, saturation and consolidation

All the marine sand was sourced from the site of the China Three Gorges New Energy Jiangsu Dafeng H8 - 2# 300 MW offshore wind farm project, which is situated in the southwestern part of the Yellow Sea, north of Maozhusha in Dafeng District, Yancheng City, Jiangsu Province. Specific details are presented in Figure 2. The offshore distance from the center of the site is 72 km, and the theoretical water depth ranges from 7.5 to 20.9 m. The sand predominantly consists of chalky sand with a shallow depth of 30 m. The sand exhibits a grey color, is saturated and loose, and contains quartz, feldspar, and a small quantity of clay in the surface layer. The primary minerals are quartz and feldspar, with occasional traces of shell debris and a small amount of clay particles. A significant amount of silt is mixed in the surface layer of some machine sites. The particles are angular, with a particle specific gravity ( $G_s$ ) of 2.70, an average particle size of 0.15 mm, an inhomogeneity coefficient of 2.11, a coefficient of curvature of 0.97, a maximum porosity ratio ( $e_{max}$ ) of 1.29, and a minimum porosity ratio ( $e_{min}$ ) of 0.63. The gradation curve is depicted in Figure 3. The *in-situ* CPTu test revealed a cone tip resistance of 5.67 MPa, a sidewall friction resistance of 35.98 kPa, and a pore water pressure of 12.5 kPa. The *in-situ* shear wave velocity was approximately 150 m/s, and there seems to be an error in the repeated statement “the *in-situ* shear wave velocity was about 1.5 kPa” which is ignored as it likely contradicts the previous velocity value.

The specimen was a hollow cylinder with an outer diameter of 100 mm, inner diameter of 60 mm, and height of 200 mm. To ensure uniformity of specimen preparation, the layer-by-layer vibration compaction method was employed. The specimen was compacted in five layers. For each layer, the required mass of particles for each grain size fraction was calculated according to the gradation, weighed separately, uniformly mixed, and then slowly poured into the mold. Subsequently, each layer was compacted to the target layer height using a compaction hammer. The drop hammer had a mass of 1 kg and a free fall height of 15 cm. Saturation of the specimen was achieved through a three-step procedure: 1) CO<sub>2</sub> flushing: carbon



dioxide (CO<sub>2</sub>) was percolated through the specimen for 15 min to displace the air. 2) De-aired water percolation: de-aired water was then flushed from the bottom to the top of the specimen until no air bubbles were observed exiting the top. 3) Stepwise back-pressure saturation: back pressure was applied incrementally in stages. Following the stepwise back-pressure saturation, the pore pressure coefficient B was measured. A specimen was deemed saturated if the measured B-value exceeded 0.95. The saturated specimen was then subjected to isotropic consolidation under an initial effective confining pressure  $\sigma_{3c}'$  of 100 kPa.

### 2.3 Test program

The controlled loading path traces an ellipse in the  $[\tau_{z\theta}, (\sigma_z - \sigma_\theta)/2]$  stress space. This path achieves a stress variation pattern characterized by continuous rotation of the principal stress axes, where the normal deviatoric stress, shear stress, and resultant generalized deviatoric stress (composed of both components) all undergo cyclic variations. As illustrated in Figure 4, the shape of this elliptical stress path is primarily defined by three key parameters: the major axis (*b*), the ratio of minor axis to major axis (*a/b*), and

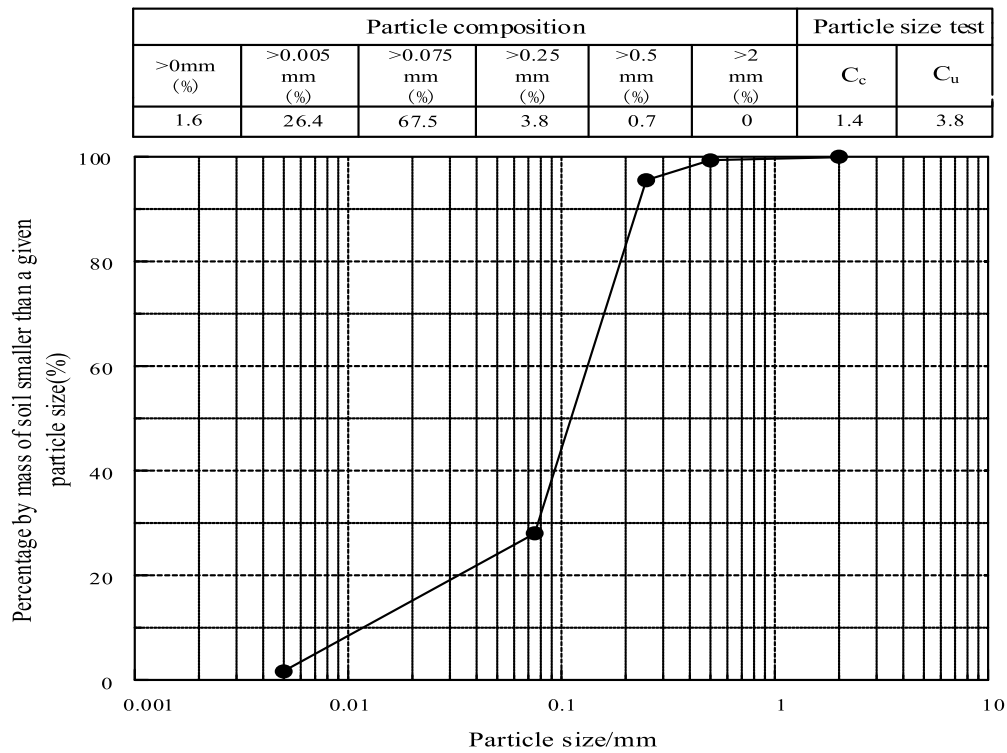


FIGURE 3 Particle grading curves of marine sands.

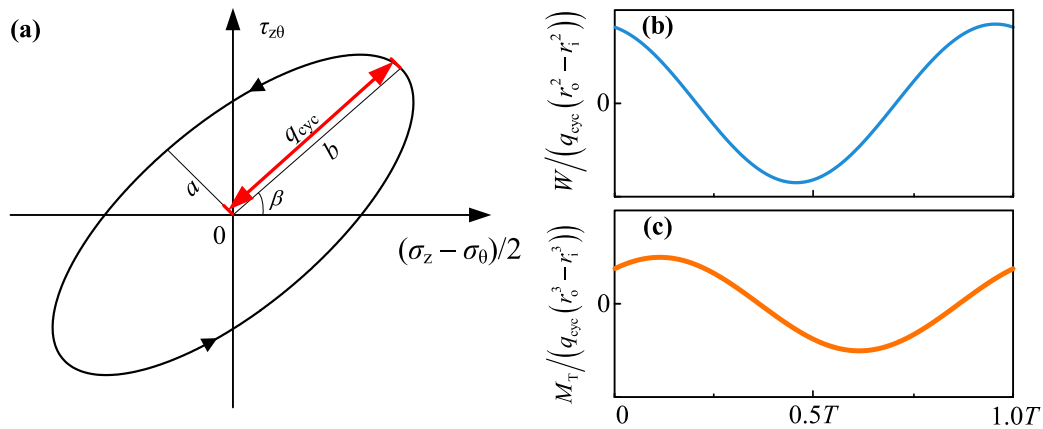


FIGURE 4 Schematic illustration of the typical loading path in testing. (a)  $\tau_{z\theta}/(\sigma_z - \sigma_\theta)/2$ . (b)  $W/(q_{cyc}(\gamma_0^2 - \gamma_1^2))/T$ . (c)  $M_T/(q_{cyc}(\gamma_0^3 - \gamma_1^3))/T$ .

the inclination angle ( $\beta$ ). Once these three characteristic parameters are specified, the stress path is uniquely defined. When  $a = 0$ , the ellipse degenerates into an inclined straight line. When  $a = b$ , the ellipse evolves into a circle.

To systematically investigate the influence of density state and stress path on the dilative behavior of saturated Nanjing fine sand, the relative density ( $D_r$ ) of the sand was categorized into three levels: 35%, 50%, and 70%, corresponding to loose, medium-dense, and dense states, respectively. For specimens sharing the

same  $D_r$  value, cyclic elliptical stress paths with different cyclic stress ratio ( $CSR = q_{cyc}/\sigma_{3c}'$ ),  $a/b$ ,  $\beta$  were applied. The loading frequency was maintained at 0.1 Hz. The loading frequency was maintained at 0.1 Hz. This frequency was selected for three primary reasons to ensure both representativeness and experimental validity: 1) It falls within the central range of typical wave loading frequencies (0.05–0.2 Hz) observed in offshore environments, thereby representing common storm-wave conditions; 2) It ensures fully drained conditions throughout the cyclic tests, allowing pore

TABLE 1 Drained bi-direction cyclic loading test scheme.

Specimen ID	$D_r = 35\%$			Specimen ID	$D_r = 50\%$			Specimen ID	$D_r = 70\%$		
	$a/b$	$\beta/^\circ$	CSR		$a/b$	$\beta/^\circ$	CSR		$a/b$	$\beta/^\circ$	CSR
E-35-1.0-45-0.15	1.0	45	0.15	E-50-1.0-45-0.15	1.0	45	0.15	E-70-1.0-45-0.15	1.0	45	0.15
E-35-1.0-45-0.20	1.0	45	0.20	E-50-1.0-45-0.20	1.0	45	0.20	E-70-1.0-45-0.20	1.0	45	0.20
E-35-1.0-45-0.25	1.0	45	0.25	E-50-1.0-45-0.25	1.0	45	0.25	E-70-1.0-45-0.25	1.0	45	0.25
E-35-1.0-45-0.30	1.0	45	0.30	E-50-1.0-45-0.30	1.0	45	0.30	E-70-1.0-45-0.30	1.0	45	0.30
E-35-0.5-30-0.15	0.5	30	0.15	E-50-0.5-30-0.15	0.5	30	0.15	E-70-0.5-30-0.15	0.5	30	0.15
E-35-0.5-45-0.15	0.5	45	0.15	E-50-0.5-45-0.15	0.5	45	0.15	E-70-0.5-45-0.15	0.5	45	0.15
E-35-0.5-60-0.15	0.5	60	0.15	E-50-0.5-60-0.15	0.5	60	0.15	E-70-0.5-60-0.15	0.5	60	0.15
E-35-0.5-30-0.20	0.5	30	0.20	E-50-0.5-30-0.20	0.5	30	0.20	E-70-0.5-30-0.20	0.5	30	0.20
E-35-0.5-45-0.20	0.5	45	0.20	E-50-0.5-45-0.20	0.5	45	0.20	E-70-0.5-45-0.20	0.5	45	0.20
E-35-0.5-60-0.20	0.5	60	0.20	E-50-0.5-60-0.20	0.5	60	0.20	E-70-0.5-60-0.20	0.5	60	0.20
E-35-0.5-30-0.25	0.5	30	0.25	E-50-0.5-30-0.25	0.5	30	0.25	E-70-0.5-30-0.25	0.5	30	0.25
E-35-0.5-45-0.25	0.5	45	0.25	E-50-0.5-45-0.25	0.5	45	0.25	E-70-0.5-45-0.25	0.5	45	0.25
E-35-0.5-60-0.25	0.5	60	0.25	E-50-0.5-60-0.25	0.5	60	0.25	E-70-0.5-60-0.25	0.5	60	0.25
E-35-0.5-30-0.30	0.5	30	0.30	E-50-0.5-30-0.30	0.5	30	0.30	E-70-0.5-30-0.30	0.5	30	0.30
E-35-0.5-45-0.30	0.5	45	0.30	E-50-0.5-45-0.30	0.5	45	0.30	E-70-0.5-45-0.30	0.5	45	0.30
E-35-0.5-60-0.30	0.5	60	0.30	E-50-0.5-60-0.30	0.5	60	0.30	E-70-0.5-60-0.30	0.5	60	0.30
E-35-0.0-45-0.15	0.0	45	0.15	E-50-0.0-45-0.15	0.0	45	0.15	E-70-0.0-45-0.15	0.0	45	0.15
E-35-0.0-45-0.20	0.0	45	0.20	E-50-0.0-45-0.20	0.0	45	0.20	E-70-0.0-45-0.20	0.0	45	0.20
E-35-0.0-45-0.25	0.0	45	0.25	E-50-0.0-45-0.25	0.0	45	0.25	E-70-0.0-45-0.25	0.0	45	0.25
E-35-0.0-45-0.30	0.0	45	0.30	E-50-0.0-45-0.30	0.0	45	0.30	E-70-0.0-45-0.30	0.0	45	0.30

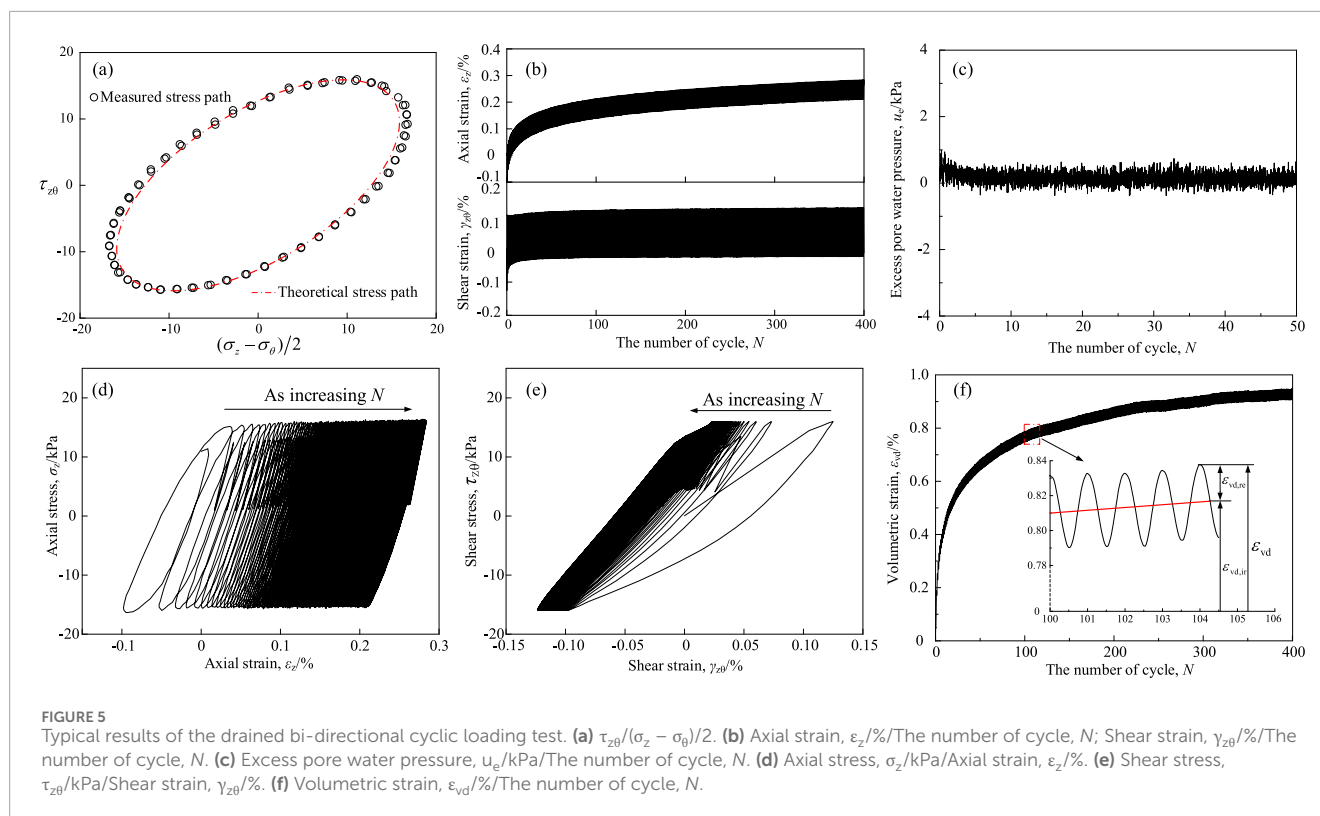
water to freely flow without generating excess pore pressure, which is crucial for accurately isolating the mechanical response of the soil skeleton; and 3) It is compatible with the dynamic performance characteristics of the HCA system and aligns with the study’s focus on long-term cumulative deformation rather than transient dynamic response. Where  $q_{cyc} = \sqrt{\tau^2 + (\sigma_v - \sigma_\theta)^2}/4|_{max}$  is the cyclic deviatoric stress amplitude. In coupled axial-torsional cyclic loading tests,  $q_{cyc}$  is conventionally employed to represent the deviatoric stress amplitude, describing the variation in the magnitude of the deviatoric stress. Its physical meaning corresponds to the major axis length of the elliptical stress path. The specific experimental program is summarized in Table 1. Specimen ID were designated according to the following naming convention:  $E-D_r-a/b-\beta-CSR$ .

### 3 Test results and discoveries

#### 3.1 Analysis of typical test results subjected to complex cyclic loading

To elucidate the mechanism of volumetric strain accumulation under complex cyclic loading, a detailed analysis of the stress-strain response is first presented. The following typical results not only demonstrate the apparatus’s capability to replicate prescribed stress paths but also provide the foundational data for understanding the subsequent decomposition of volumetric strain into reversible and irreversible components, as well as the influence of stress path.

Figure 5 presents typical test results of marine sand under cyclic elliptical stress paths, including: comparison of measured versus



theoretical stress paths in the  $[\tau_{z0}, (\sigma_z - \sigma_0)/2]$  stress space; time histories of axial strain ( $\epsilon_z$ ), shear strain ( $\gamma_{z0}$ ), and excess pore water pressure ( $u_e$ ); hysteretic loops of  $\sigma_z$  versus  $\epsilon_z$ ; hysteretic loops of  $\tau_{z0}$  versus  $\gamma_{z0}$ ; time history of volumetric strain ( $\epsilon_{vd}$ ). The following observations can be drawn from Figure 5: (a) The HCA instrument demonstrated its capability to accurately simulate the prescribed coupled cyclic stress paths; (b) The  $\sigma_z$ - $\epsilon_z$  relationship exhibited distinct hysteretic loops, these loops were initially unclosed, indicating significant plastic deformation occurred during the early loading cycle; (c) as the number of cycles ( $N$ ) increased, the hysteretic loops transitioned from unclosed to closed, and their enclosed area progressively decreased. This evolution signifies the soil approaching a critical state; (d) throughout the test, the  $\epsilon_z$  development with increasing  $N$  comprised two distinct phases: a phase of rapid growth followed by a phase of stable accumulation. This behavior is primarily attributed to changes in the irreversible dilative component during the initial  $N$ ; (e) during the coupled axial-torsional cyclic loading, the  $u_e$  value of the specimen consistently remained within the range of 0 ~ 1 kPa. No significant accumulation of  $u_e$  was observed, indicating that pore water could freely flow into or drain out of the specimen.

The observed stress-strain responses, particularly the evolution of hysteretic loops and the development of axial strain, are direct manifestations of the underlying “intrinsically consistent physical mechanism” mentioned in the introduction, which couples shear deformation with volumetric change. The following decomposition of total volumetric strain into reversible and irreversible components allows for a more direct examination of this coupling effect under complex stress paths. The cyclic volumetric strain is defined as half the difference between the maximum and minimum volumetric

strain ( $\epsilon_{vd}$ ) values within a single cycle (Xu et al., 2025), and the accumulated volumetric strain is defined as the average of the maximum and minimum  $\epsilon_{vd}$  values within a cycle. As evident in Figure 5,  $\epsilon_{vd}$  comprises a reversible cyclic strain component ( $\epsilon_{vd,rc}$ ) and an irreversible accumulated strain component ( $\epsilon_{vd,ir}$ ). This decomposition aligns with the experimental findings of Zhang, (2000), Duku et al. (2008), and Wichtmann et al. (2005). The reversible component ( $\epsilon_{vd,rc}$ ) is elastic in nature and does not induce changes in the effective stress state of the soil. For soil dynamics characteristics, the focus is often on permanent deformations and accumulated pore water pressure, which are intrinsically linked to the irreversible accumulated strain component ( $\epsilon_{vd,ir}$ ). Therefore, the primary investigation centers on the influence of density state and stress path on  $\epsilon_{vd,ir}$  for the saturated sand. Key experimental findings as following: 1)  $\epsilon_{vd,ir}$  is irrecoverable, representing plastic deformation.  $\epsilon_{vd,ir}$  consistently manifested as monotonic volume compression; 2) By convention,  $\epsilon_{vd,ir}$  is defined as negative during dilation and positive during contraction; 3) The increasing rate of  $\epsilon_{vd,ir}$  was highest during the initial stages of cyclic loading. Furthermore, the maximum rate of change within each half-cycle consistently occurred at the point of shear stress reversal; 4) The increasing rate of  $\epsilon_{vd,ir}$  progressively diminished with increasing  $N$ , asymptotically approaching zero as the soil reached the critical state.

To further investigate the differences in  $\epsilon_{vd}$  increments of saturated marine fine sand under various cyclic stress paths induced by wave loading, supplementary tests were conducted on saturated marine fine sand with  $D_r = 50\%$ . These included pure cyclic compression-tension loading test and pure cyclic torsional loading test, both controlled at a CSR of 0.20. Figure 6 presents the relationships between  $\epsilon_{vd}$  and  $N$  for the specimens under pure

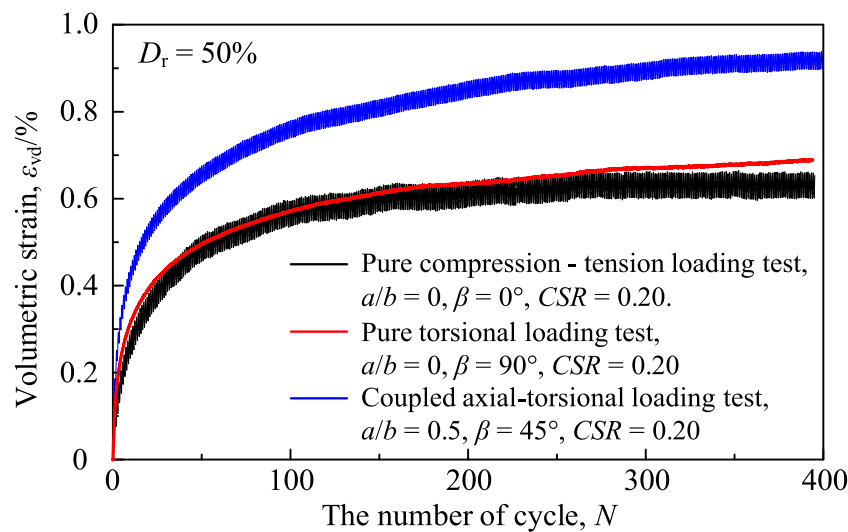


FIGURE 6  
Volumetric strain time-histories of the saturated sands under different cyclic stress paths.

compression-tension loading, pure torsional loading, and coupled axial-torsional loading. The following key observations are drawn from the figure: consistent with the behavior observed under coupled axial-torsional loading,  $\varepsilon_{vd,ir}$  under both pure compression-tension loading and pure torsional loading increased with  $N$ . Furthermore, the increasing rate of  $\varepsilon_{vd,ir}$  first decrease rapidly as  $N$  increases, and then gradually approach 0. At an identical CSR, the development of  $\varepsilon_{vd,ir}$  with increasing  $N$  was essentially consistent between the two simple stress paths (pure compression - tension and pure torsion). The magnitude of  $\varepsilon_{vd,ir}$  developed under the complex stress path (coupled axial-torsional loading) was significantly greater than that developed under either simple stress path. This finding indicates that previous experimental studies based solely on simple stress paths (either pure compression-tension or pure torsion) underestimated the development of  $\varepsilon_{vd,ir}$  in saturated marine sand. Additionally,  $\varepsilon_{vd,re}$  under pure compression-tension loading was slightly greater than that observed under coupled axial-torsional loading. The value of  $\varepsilon_{vd,re}$  under pure torsional loading remained essentially zero. This behavior arises because  $\varepsilon_{vd,re}$  is induced by the periodically varying mean effective stress, which is present in pure compression-tension loading but absent in pure torsion (where mean effective stress remains constant).

### 3.2 Volumetric strain accumulation characteristics and influencing factors

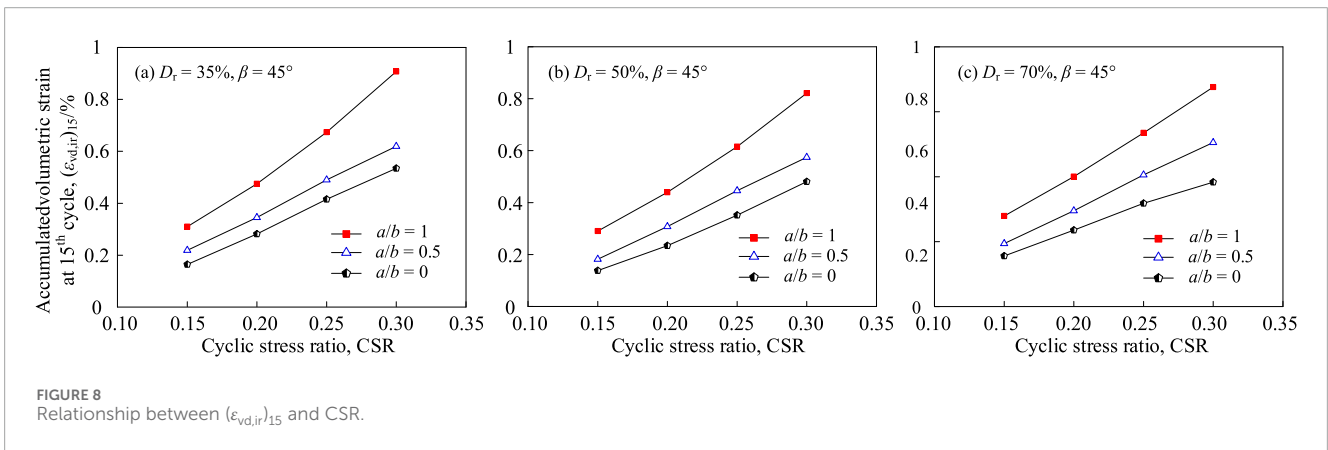
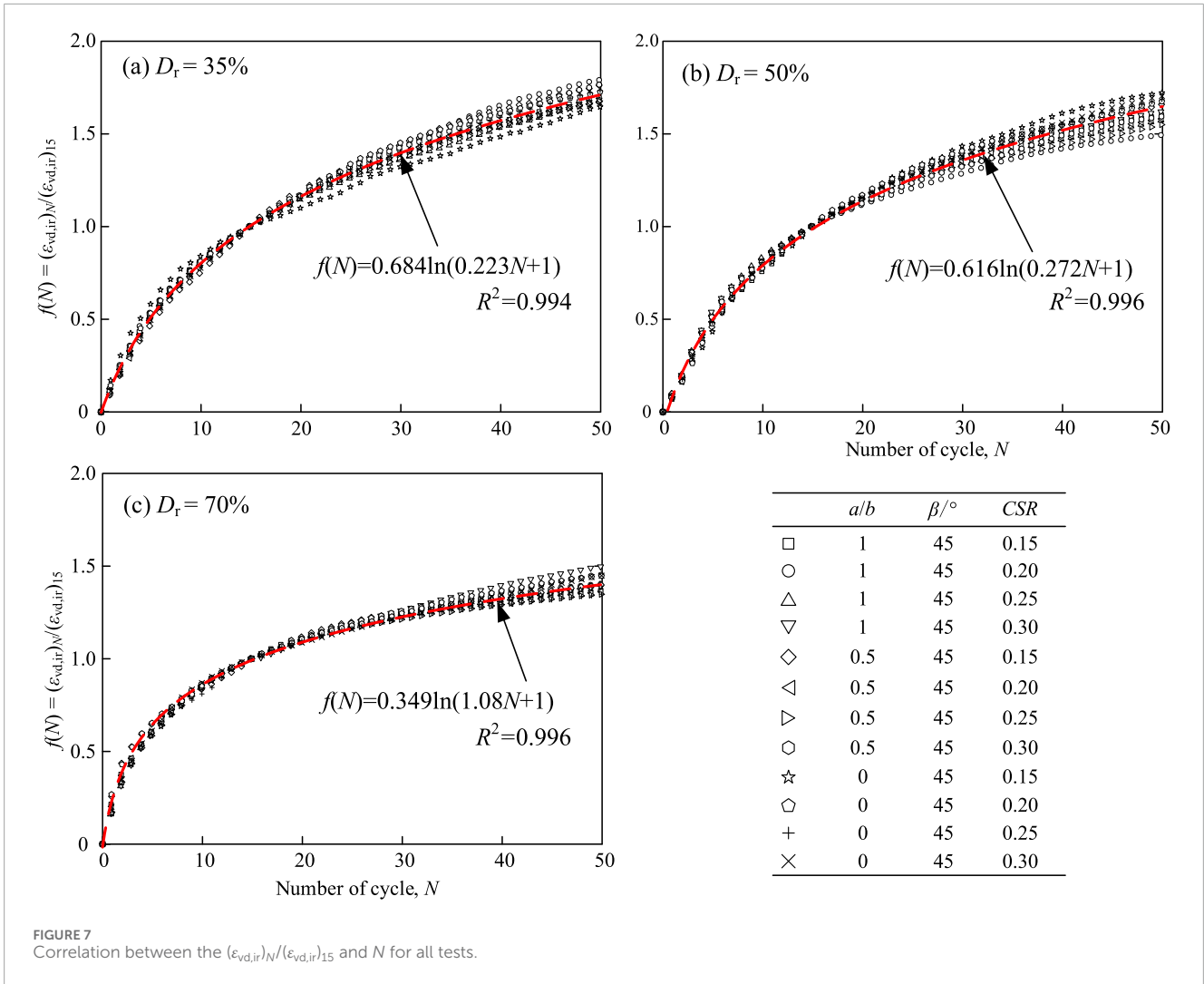
Conventionally, in the estimation of site settlement induced by earthquake ground motions, the accumulated volumetric strain at  $N = 15$ , denoted as  $(\varepsilon_{vd,ir})_{15}$ , is used to approximate the settlement for an earthquake magnitude of  $M = 7.5$  (Duku et al., 2008). This convention provides a well-established and widely understood reference point for characterizing strain accumulation under cyclic loading. Beyond its seismic origin, the parameter  $(\varepsilon_{vd,ir})_{15}$  has proven to be an effective and stable normalization benchmark in

various cyclic loading studies, as it captures a representative stage of strain development while minimizing the influence of early-cycle variability. Furthermore, in view of the effectiveness and applicability of  $(\varepsilon_{vd,ir})_{15}$  in the normalizing the volumetric strain accumulation characteristics of soil subjected to cyclic loading (Duku et al., 2008; Yee et al., 2014; Tokimatsu and Seed, 1987), the accumulated volumetric strain at the 15th cycle  $(\varepsilon_{vd,ir})_{15}$  is analyzed herein to investigate the  $\varepsilon_{vd,ir}$  development in marine sand subjected to wave-induced complex cyclic loading. Figure 7 presents the relationship curves between the  $(\varepsilon_{vd,ir})_N/(\varepsilon_{vd,ir})_{15}$  and  $N$  for various test conditions. The results demonstrate that: for specimens with identical  $D_r$ , the  $(\varepsilon_{vd,ir})_N/(\varepsilon_{vd,ir})_{15}$  values under different complex stress paths are distributed within a relatively narrow band as  $N$  increases. This observation indicates that the influence of stress path on  $(\varepsilon_{vd,ir})_N/(\varepsilon_{vd,ir})_{15}$  is relatively minor. Consequently, the analysis can focus primarily on the relationship between  $(\varepsilon_{vd,ir})_N/(\varepsilon_{vd,ir})_{15}$  and  $N$ . The  $(\varepsilon_{vd,ir})_N/(\varepsilon_{vd,ir})_{15}$  be reasonably and simply expressed as a logarithmic function of  $N$ :

$$f(N) = (\varepsilon_{vd,ir})_N/(\varepsilon_{vd,ir})_{15} = C_2 \ln [C_1 N + 1] \quad (1)$$

where  $C_1$  and  $C_2$  are fitting parameters.

As can be seen from the above, for the given  $D_r$ ,  $(\varepsilon_{vd,ir})_{15}$  is the key parameter characterizing the volumetric strain accumulation characteristics of saturated marine sands. Figure 8 presents the relationship between  $(\varepsilon_{vd,ir})_{15}$  and CSR for saturated marine sands. The figure reveals that CSR significantly influences the development of  $(\varepsilon_{vd,ir})_{15}$ . For specimens with given  $a/b$ ,  $\beta$ , and  $D_r$ ,  $(\varepsilon_{vd,ir})_{15}$  increases rapidly with increasing CSR. However, for specimens sharing the same  $D_r$ , identical CSR, and identical  $\beta$ , the magnitude of  $(\varepsilon_{vd,ir})_{15}$  increases with increasing  $a/b$ . Furthermore, the influence of  $a/b$  cannot be normalized into a unified pattern across the CSR vs.  $(\varepsilon_{vd,ir})_{15}$  relationship curves. This behavior stems from the fact that CSR solely characterizes the variation in deviatoric stress amplitude (represented by the semi-major axis length of the ellipse) but fails to adequately capture changes in the shape of the stress path, such



as the minor-to-major axis ratio ( $a/b$ ). The deformation of the specimen is essentially induced by the coupled action of the axial stress amplitude and the shear stress amplitude. For coupled axial-torsional cyclic loading tests sharing the same  $b$  value but differing in  $a/b$ , the applied stress paths differ, consequently leading to distinct shearing effects (e.g., differences in non-coaxiality).

Figure 9 illustrates the influence of  $\beta$  on  $(\epsilon_{vd,ir})_{15}$  at a constant CSR. As shown,  $\beta$  has no significant effect on  $(\epsilon_{vd,ir})_{15}$ ; that is, once CSR falls below a specific threshold value,  $(\epsilon_{vd,ir})_{15}$  becomes virtually independent of  $\beta$ . For marine sand under different  $D_r$  values, this threshold CSR value is approximately 0.20. This finding aligns with Xu et al. (2014), who likewise observed no

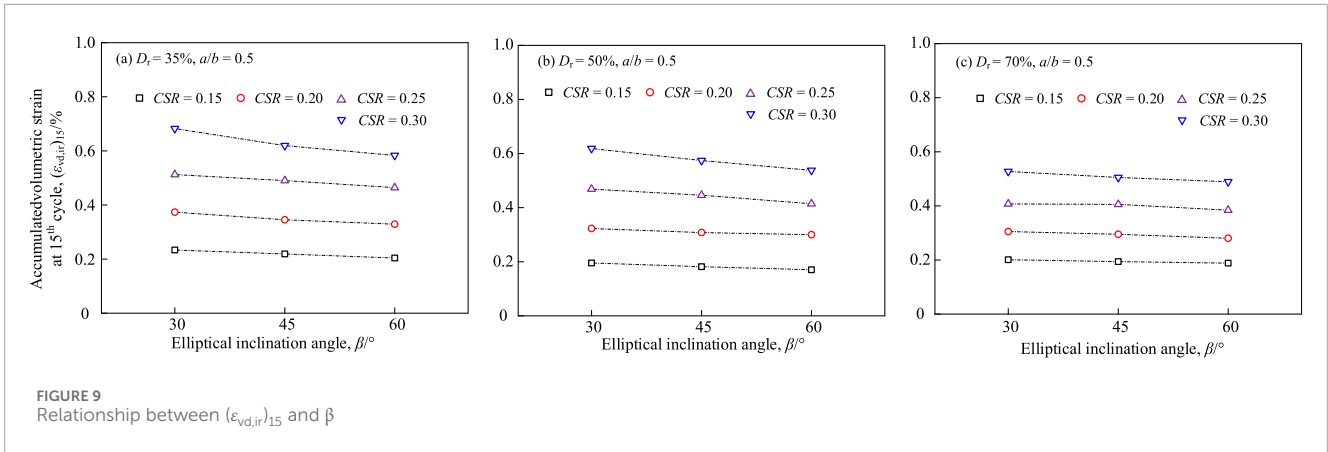


FIGURE 9 Relationship between  $(\epsilon_{vd,ir})_{15}$  and  $\beta$

significant influence of the elliptical inclination angle  $\beta$  on the cyclic resistance.

The preceding experimental results demonstrate the limitations of CSR when used to analyze coupled cyclic loading tests, specifically its inability to adequately represent the effective stress level experienced by soil elements undergoing continuous principal stress rotation. To address this, (Huang et al., 2015). [29] proposed the term Equivalent cyclic stress ratio (ESR) to characterize the magnitude of cyclic stress under complex stress paths, ESR serves as a more comprehensive index than CSR, as it integrates both the axial and shear stress amplitudes over the entire elliptical path, thereby better representing the effective cyclic stress level under conditions of principal stress rotation. ESR is defined as Equation 2:

$$ESR = q_{equ} / \sigma'_{3c}$$

$$q_{equ} = \frac{1}{T} \int_0^T |q(t)| dt = \frac{1}{T} \int_0^T \sqrt{\tau^2 + \left(\frac{\sigma_v - \sigma_\theta}{2}\right)^2} dt \quad (2)$$

Where,  $T$  represents the cyclic loading period,  $|q(t)|$  denotes the distance from any point on the stress path to the origin. Thus,  $q_{equ}$  physically represents the average intensity of cyclic loading, defined as the mean value of the maximum cyclic shear stress experienced by the soil element. For elliptical stress paths, the equivalent cyclic stress  $q(t)$  and  $q_{equ}$  can be explicitly expressed as Equation 3:

$$q(t) = \sqrt{\left(\tau_d \cdot \sin\left(\frac{2\pi}{T}t\right)\right)^2 + \left(\frac{\sigma_d}{2} \cdot \cos\left(\frac{2\pi}{T}t + \varphi\right)\right)^2}$$

$$q_{equ} = \frac{1}{T} \int_0^T |q(t)| dt = (0.64 \sim 1) q_{cyc} \quad (3)$$

Where,  $\tau_d$  is the cyclic shear stress amplitude,  $\sigma_d$  is the cyclic axial stress amplitude. For elliptical stress paths where  $q_{equ}$  cannot be obtained through direct integration, numerical integration methods may be employed for its evaluation.

Figure 10 illustrates the relationship between  $(\epsilon_{vd,ir})_{15}$  and ESR for specimens with various  $D_r$ . For given  $D_r$ , regardless of whether the stress paths are identical, the  $(\epsilon_{vd,ir})_{15}$  values of saturated sand with different ESR values are distributed within a narrow band. Moreover,  $(\epsilon_{vd,ir})_{15}$  increases linearly with rising ESR, demonstrating a strong correlation. This indicates that ESR can serve as a characteristic parameter to effectively describe complex stress

paths involving principal stress axis rotation. At the same  $D_r$ , ESR can ideally characterize the  $(\epsilon_{vd,ir})_{15}$  under different stress paths:

$$(\epsilon_{vd,ir})_{15} = C_3 (ESR - ESR_t) \quad (4)$$

where  $C_3$  are fitting parameter. In addition, as shown in Figure 10, saturated marine sand exhibits a distinct volumetric threshold cyclic stress ratio  $ESR_t$ . When ESR is below  $ESR_t$ , no  $\epsilon_{vd,ir}$  develops; once ESR exceeds this threshold, the  $\epsilon_{vd,ir}$  increases rapidly with further increases in ESR. The pore pressure ratio under undrained conditions shares the same physical basis as the volumetric strain under drained conditions. Therefore,  $ESR_t$  is of significant importance for understanding and addressing geodynamic problems induced by cyclic loading, such as seismic excitation, ocean wave action, and pile-driving vibrations. Ivsic (2006) and Park et al. (2015) suggested that the threshold cyclic stress ratio can be determined based on the threshold shear strain ( $\gamma_{tv}$ ). For saturated sand, the  $\gamma_{tv}$  ranges from 0.014% to 0.023%, corresponding to  $ESR_t = 0.05$  to 0.06.

## 4 A new stress-dependent accumulated volumetric strain incremental model

Under cyclic loading, the accumulated volumetric deformation of cohesionless soil under fully drained conditions shares the same physical mechanism as the generation of excess pore pressure under undrained conditions. An accurate and efficient accumulated volumetric strain incremental model represents a key scientific issue for the investigation of dynamic response characteristics and stability assessment of marine engineering structures—such as offshore wind turbines, oil platforms, and subsea pipelines and cables—in complex multi-hazard environments involving waves, tsunamis, storm surges, or earthquakes. By combining Equations 1, 4, it can be obtained:

$$(\epsilon_{vd,ir})_N = C_3 \cdot C_2 \ln [C_1 N + 1] \cdot \lambda \quad (5)$$

Differentiating Equation 5 with respect to  $N$  yields the parametric expression for volumetric strain increment:

$$\frac{\Delta \epsilon_{vd,ir}}{\lambda} = C_1 C_2 C_3 \cdot \exp\left(-\frac{1}{C_2 C_3} \frac{\epsilon_{vd,ir}}{\lambda}\right) \quad (6)$$

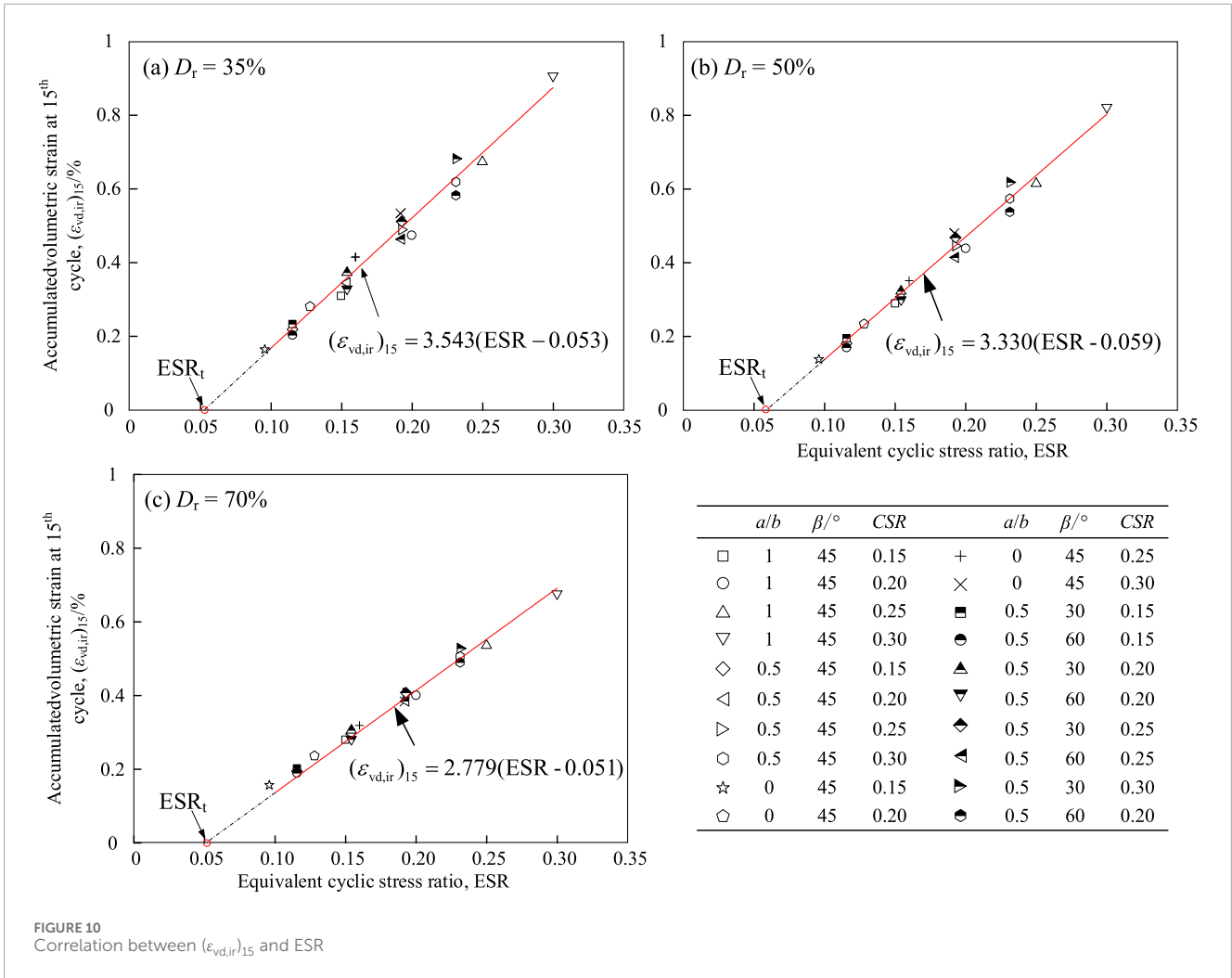


FIGURE 10 Correlation between  $(\epsilon_{vd,ir})_{15}$  and ESR

In Equation 6 letting  $k_1 = C_1 C_2 C_3$  and  $k_2 = 1/(C_2 C_3)$ , it can be obtained that:

$$\frac{\Delta \epsilon_{vd,ir}}{\lambda} = k_1 \cdot \exp\left(-k_2 \frac{\epsilon_{vd,ir}}{\lambda}\right) \quad (7)$$

Where:

$$\lambda = ESR - ESR_t \quad (8)$$

The model requires only two parameters  $k_1$  and  $k_2$ . Analysis reveals that  $k_1$  and  $k_2$  exhibit strong dependence on  $D_r$ . To establish a more precise relationship between  $k_1$ ,  $k_2$  and  $D_r$ , three additional tests were conducted on saturated marine sand at  $D_r = 60\%$ , with specific test conditions detailed in Table 2. Figure 11 presents the relationship curves between  $k_1$ ,  $k_2$  and  $D_r$ . As illustrated, both  $k_1$  and  $k_2$  demonstrate rapid increase with growing  $D_r$ . For the tested sand,  $k_1$  and  $k_2$  can be expressed as power functions of  $D_r$ :

$$k_1 = 2.143(D_r)^{2.904} + 0.469, R^2 = 0.975 \quad (9)$$

$$k_2 = 3.419(D_r)^{3.982} + 0.358, R^2 = 0.993 \quad (10)$$

Therefore, combine Equations 7–10, a stress-dependent model can be established to characterize the accumulated volumetric strain

TABLE 2 Cases of supplementary test.

Specimen ID	$D_r/\%$	<i>a/b</i>	$\beta/^\circ$	CSR
E-60-0.0-45-0.20	60	1.0	45	0.15
E-60-0.5-45-0.20	60	1.0	45	0.20
E-60-1.0-45-0.20	60	1.0	45	0.25

development characteristics of saturated marine sands subjected to wave-induced complex cyclic loading.

Byrne (1991) modified the strain-dependent accumulated volumetric strain increment model originally proposed by Martin et al. (1975) into an exponential function form. This refined model contains only two parameters with more explicit physical significance, and has been extensively applied in effective stress dynamic analysis methods (Azadi et al., 2010; Long et al., 2013; Zhao et al., 2017).

$$\frac{\Delta \epsilon_{vd}}{\gamma} = m_1 \cdot \exp\left(-m_2 \frac{\epsilon_{vd}}{\gamma}\right) \quad (11)$$

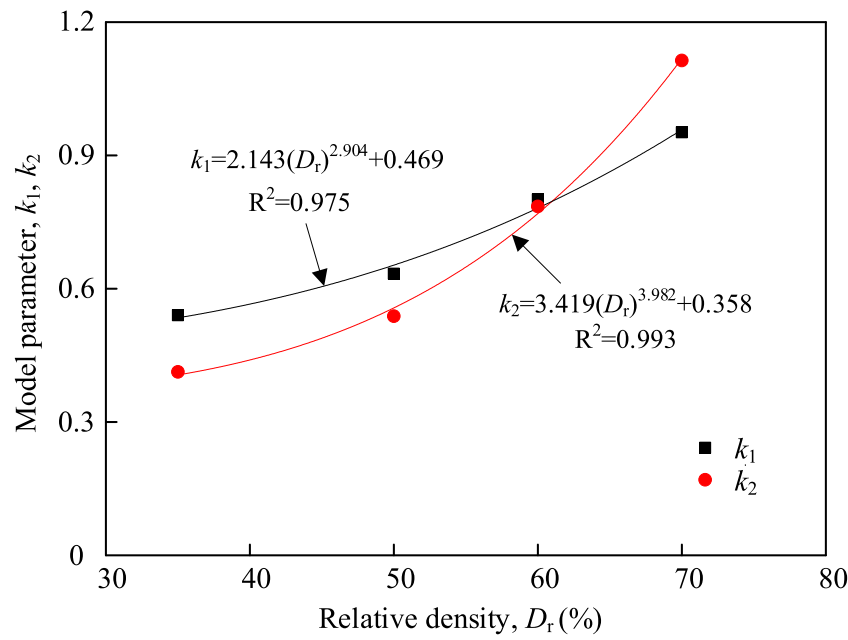


FIGURE 11 Relationships between  $k_1$ ,  $k_2$  and  $D_r$ .

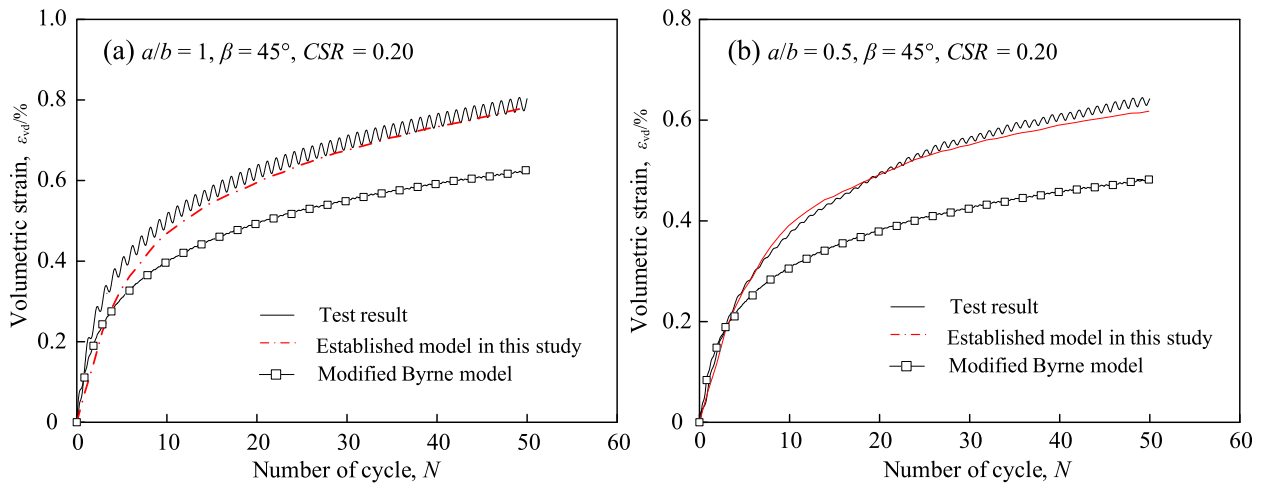


FIGURE 12 Comparison between the measured and predicted volumetric strain time-histories based on different models.

Based on Byrne model (Equation 11) and incorporating results from strain-controlled drained/undrained multistage and single-stage cyclic triaxial tests, Chen et al. (2019) developed a modified Byrne model suitable for saturated continental sand subjected to conventional cyclic loading, the modified strain-dependent Byrne model is expressed as follows:

$$\frac{\Delta \epsilon_{vd}}{(y - 0.02)^{0.125}} = m_1 \cdot \exp \left[ -m_2 \frac{\epsilon_{vd}}{(y - 0.02)^{0.125}} \right] \quad (12)$$

Where  $m_1 = 7.05(D_r)^{-0.5}$ ,  $m_2 = 0.15/m_1$ .

The modified strain-dependent volumetric strain increment model proposed by Chen et al. (2019) (Equation 12) and the

stress-dependent accumulated volumetric strain incremental model (Equations 5, 7 and 8) established in this study were respectively employed to predict the accumulated volumetric strain development of saturated marine sand ( $D_r = 60\%$ ) under complex cyclic loading conditions. The comparative results are presented in Figure 12. As shown, the predictions from the modified Byrne model underestimate the experimental measurements, whereas the stress-dependent model established in this study demonstrates significantly better agreement with the experimental data. This discrepancy arises because the modified Byrne model was developed based on direct shear test data, which cannot adequately capture the coupled effects of axial stress amplitude

TABLE 3 Quantitative error analysis of model predictions.

Test case (specimen ID)	Proposed stress-dependent model		Modified byrne model	
	R <sup>2</sup>	RMSE (×10 <sup>-3</sup> )	R <sup>2</sup>	RMSE (×10 <sup>-3</sup> )
E-35-1.0-45-0.20	0.978	1.05	0.885	2.98
E-35-0.5-60-0.25	0.981	1.12	0.901	2.76
E-50-0.0-45-0.15	0.983	0.92	0.908	2.15
E-50-1.0-45-0.30	0.972	1.34	0.879	3.22
E-50-0.5-30-0.20	0.985	0.89	0.915	2.08
E-70-0.5-45-0.25	0.989	0.74	0.924	1.95
E-70-1.0-45-0.20	0.991	0.68	0.931	1.82
Mean (all cases)	0.983	0.95	0.907	2.42
Standard deviation	0.007	0.22	0.018	0.45

and shear stress amplitude variations on soil volumetric strain development.

To comprehensively evaluate the predictive accuracy and robustness of the proposed stress-dependent model, its performance was compared with the modified Byrne model across multiple representative test conditions. These conditions were selected to cover a range of relative densities ( $D_r$ ), stress path shapes (a/b), inclination angles ( $\beta$ ), and cyclic stress ratios (CSR). The coefficient of determination ( $R^2$ ) and the root mean square error (RMSE) were calculated for each case. The results are summarized in Table 3.

As summarized in Table 3, the proposed stress-dependent model consistently achieves superior predictive accuracy across all test conditions. It exhibits higher  $R^2$  values (closer to 1) and significantly lower RMSE values compared to the modified Byrne model. The proposed model's performance is also more stable, as indicated by its lower standard deviations for both  $R^2$  (0.007 vs. 0.018) and RMSE ( $0.22 \times 10^{-3}$  vs.  $0.45 \times 10^{-3}$ ). This comprehensive quantitative assessment confirms the robustness and reliability of the proposed model for predicting volumetric strain accumulation under a wide spectrum of wave-induced complex cyclic loading conditions.

## 5 Conclusion

This study systematically conducted axial-torsional coupled cyclic shear tests on saturated marine sand under wave-induced complex cyclic loading to investigate its cumulative volumetric strain behaviour, and a corresponding stress-dependent incremental cumulative volumetric strain model was established, the conclusion is as follows:

1. This study elucidated the physical mechanism governing volume strain accumulation in saturated marine sand under complex stress paths induced by wave action. Experimental findings demonstrated that conventional models based on

uniaxial loading significantly underestimate actual volume strain accumulation due to their failure to account for the continuous rotation of principal stress axes and stress coupling effects.

2. Research has revealed that when cumulative strain is normalised to the strain value at week 15, the normalised strain under different stress paths converges towards a unified logarithmic function relationship with the progression of cycle counts. This normalisation pattern exhibits minimal influence from stress paths, providing direct justification for simplifying engineering models with complex wave load histories and predicting long-term deformation.
3. To overcome the limitations of the conventional cyclic stress ratio (CSR) in characterising coupled amplitude-path behaviour, this study proposes the equivalent cyclic stress ratio (ESR). By integrating stress ellipse strength, ESR provides a unified characterisation of volume strain accumulation patterns across different ellipse shapes (a/b) and inclination angles ( $\beta$ ), while identifying a stress threshold for volume strain accumulation ( $ESR_t \approx 0.05-0.06$ ).
4. Based on ESR, this study established a stress-dependent volumetric change increment model requiring only two parameters related to relative density. Validation demonstrated that this model significantly outperforms the modified Byrne model based on direct shear tests in predicting volumetric change development under coupled loading, providing a more reliable tool for assessing long-term settlement of marine engineering foundations.

## Data availability statement

The raw data supporting the conclusions of this article will be made available by the authors, without undue reservation.

## Author contributions

YW: Methodology, Writing – review and editing, Writing – original draft. ZZ: Validation, Writing – review and editing, Writing – original draft. QW: Methodology, Writing – review and editing, Data curation. GX: Investigation, Conceptualization, Formal analysis, Writing – review and editing. GC: Writing – review and editing, Investigation, Conceptualization.

## Funding

The author(s) declared that financial support was not received for this work and/or its publication.

## Conflict of interest

YW was employed by China Oilfield Services Ltd. (COSL Geophysical, Marine Survey and Geotech Company). Author GX was employed by Zhejiang Huadong Geotechnical Investigation & Design Institute CO, Ltd.

The remaining author(s) declared that this work was conducted in the absence of any commercial or financial

relationships that could be construed as a potential conflict of interest.

## Generative AI statement

The author(s) declared that generative AI was not used in the creation of this manuscript.

Any alternative text (alt text) provided alongside figures in this article has been generated by Frontiers with the support of artificial intelligence and reasonable efforts have been made to ensure accuracy, including review by the authors wherever possible. If you identify any issues, please contact us.

## Publisher's note

All claims expressed in this article are solely those of the authors and do not necessarily represent those of their affiliated organizations, or those of the publisher, the editors and the reviewers. Any product that may be evaluated in this article, or claim that may be made by its manufacturer, is not guaranteed or endorsed by the publisher.

## References

- Azadi, M., Mir, M., and Hosseini, S. M. (2010). Analyses of the effect of seismic behavior of shallow tunnels in liquefiable grounds. *Tunn. Undergr. Space Technol.* 25 (5), 543–552. doi:10.1016/j.tust.2010.03.003
- Byrne, P. M. (1991). "A cyclic shear-Volume coupling and pore pressure model for sand." 1991. 47–55. Available online at: <https://scholarsmine.mst.edu/icrageesd/02icrageesd/session01/1/>.
- Chen, G. X., Zhou, Z. L., Pan, H., Sun, T., and Li, X. J. (2016). The influence of undrained cyclic loading patterns and consolidation states on the deformation features of saturated fine sand over a wide strain range. *Eng. Geol.* 204, 77–93. doi:10.1016/j.enggeo.2016.02.008
- Chen, G. X., Zhao, D. F., Chen, W. Y., and Juang, C. H. (2019). Excess pore-water pressure generation in cyclic undrained testing. *J. Geotechnical Geoenvironmental Eng.* 145 (7), 04019022. doi:10.1061/(asce)gt.1943-5606.0002057
- Chen, G. X., Qin, Y., Ma, W. J., Liang, K., Wu, Q., and Juang, C. H. (2024). Liquefaction susceptibility and deformation characteristics of saturated coral sandy soils subjected to cyclic loadings—A critical review. *Earthq. Eng. Eng. Vib.* 23 (1), 261–296. doi:10.1007/s11803-024-2221-4
- Dobry, R., Pierce, W. G., Dyvik, R., Thomas, G. E., and Ladd, R. S. (1985). *Pore pressure model for cyclic straining of sand*, 6. Troy, New York: Rensselaer Polytechnic Institute.
- Duku, P. M., Stewart, J. P., Whang, D. H., and Yee, E. (2008). Volumetric strains of clean sands subject to cyclic loads. *J. Geotechnical Geoenvironmental Engineering* 134 (8), 1073–1085. doi:10.1061/(asce)1090-0241(2008)134:8(1073)
- Gutierrez, M., Ishihara, K., and Towhata, I. (1991). Flow theory for sand during rotation of principal stress direction. *Soils Foundations* 31 (4), 121–132. doi:10.3208/sandf1972.31.4\_121
- Huang, B., Chen, X. Y., and Zhao, Y. (2015). A new index for evaluating liquefaction resistance of soil under combined cyclic shear stresses. *Eng. Geol.* 199, 125–139. doi:10.1016/j.enggeo.2015.10.012
- Ishihara, K., and Towhata, I. (1983). Sand response to cyclic rotation of principal stress directions as induced by wave loads. *Soils Found.* 23 (4), 11–26. doi:10.3208/sandf1972.23.4\_11
- Iysic, T. (2006). A model for presentation of seismic pore water pressures. *Soil Dyn. Earthq. Eng.* 26, 191–199. doi:10.1016/j.soildyn.2004.11.025
- Juan, P. N., Valdecantos, N. V., and Troch, P. (2025). Advancing artificial intelligence in ocean and maritime engineering: trends, progress, and future directions. *Ocean. Eng.* 339 (P1), 122077. doi:10.1016/j.oceaneng.2025.122077
- Long, H., Chen, G. X., and Zhuang, H. Y. (2013). Effective stress analysis of seismic response characteristics of metro station structure in liquefiable foundation. *Rock Soil Mech.* 34 (06), 1731–1737. doi:10.16285/j.rsm.2013.06.014
- Martin, G. R., Finn, W. D. L., and Seed, H. B. (1975). Fundamentals of liquefaction under cyclic loading. *J. Geotechnical Eng.* 101 (5), 423–438. doi:10.1061/ajgeb6.0000164
- Miura, K., Miura, S., and Toki, S. (1986). Deformation behavior of anisotropic dense sand under principal stress axes rotation. *Soils Found.* 26 (1), 36–52. doi:10.3208/sandf1972.26.36
- Park, T., Park, D., and Ahn, J. K. (2015). Pore pressure model based on accumulated stress. *Bull. Earthq. Eng.* 13, 1913–1926. doi:10.1007/s10518-014-9702-1
- Prasanna, R., and Sivathayalan, S. (2021). A hollow cylinder torsional shear device to explore behavior of soils subjected to complex rotation of principal stresses. *Geotechnical Test. J.* 44 (6), 1595–1616. doi:10.1520/gtj20190394
- Qin, Y., Du, X. Y., Xu, Z. H., Ma, W. J., and Chen, G. X. (2024). Comparisons of cyclic response and reconsolidation volumetric strain of saturated coral sand and siliceous sand. *Mar. Georesources Geotechnol.* 42 (3), 317–326. doi:10.1080/1064119x.2023.2174462
- Symes, M. J., Gens, A., and Hight, D. W. (1988). Drained principal stress rotation in saturated sand. *Geotechnique* 38 (1), 59–81. doi:10.1680/geot.1988.38.1.59
- Tokimatsu, K., and Seed, H. B. (1987). Evaluation of settlements in sands due to earthquake shaking. *J. Geotechnical Eng.* 113 (8), 861–878. doi:10.1061/(asce)0733-9410(1987)113:8(861)
- Tong, Z. X., Zhang, J. M., Yu, Y. L., and Zhang, G. (2010). Drained deformation behavior of anisotropic sands during cyclic rotation of principal stress axes. *J. Geotechnical Geoenvironmental Eng.* 136 (11), 1509–1518. doi:10.1061/(asce)gt.1943-5606.0000378
- Wang, Z. T., Liu, P., Jeng, D., and Yang, Q. (2017). Cyclic strength of sand under a nonstandard elliptical rotation stress path induced by wave loading. *J. Hydrodynamics* 29 (1), 89–95. doi:10.1016/s1001-6058(16)60720-5
- Wichtmann, T., Niemunis, A., and Triantafyllidis, T. (2005). Strain accumulation in sand due to cyclic loading: drained triaxial tests. *Soil Dyn. Earthq. Eng.* 25 (12), 967–979. doi:10.1016/j.soildyn.2005.02.022
- Wu, Z. X., Yin, Z. Y., Dano, C., and Hicher, P. Y. (2020). Cyclic volumetric strain accumulation for sand under drained simple shear condition. *Appl. Ocean. Res.* 101, 102200. doi:10.1016/j.apor.2020.102200
- Xiong, H., Guo, L., Cai, Y., and Yang, Z. (2016). Experimental study of drained anisotropy of granular soils involving rotation of principal stress direction. *Eur. Journal Environmental Civil Engineering* 20 (4), 431–454. doi:10.1080/19648189.2015.1039662

- Xu, C. S., Gao, Y., Du, X. L., and Geng, L. (2014). Dynamic strength of saturated sand under bi-directional cyclic loading. *Chin. J. Geotechnical Eng.* 36 (12), 2335–2340.
- Xu, M., Wang, L., Chen, Z., Zhang, S., and Guo, Z. (2025). Mechanism-based modeling for interface mechanical behavior during shearing. *Acta Geotech.* 20, 1–20. doi:10.1007/s11440-025-02700-0
- Yee, E., Duku, P. M., and Stewart, J. P. (2014). Cyclic volumetric strain behavior of sands with fines of low plasticity. *J. Geotechnical Geoenvironmental Eng.* 140 (4), 04013042. doi:10.1061/(asce)gt.1943-5606.0001041
- Yuan, R., Yu, H. H., and Wang, X. W. (2024). Unified modeling for the simple shear behavior of clay and sand accounting for principal stress rotations. *Int. J. Geomechanics* 24 (11), 04024239. doi:10.1061/ijgnai.gmeng-8399
- Yue, C., Xu, C., Liang, K., and Xiuli, D. (2023). Effect of cyclic loading frequency on cyclic behaviour of saturated sand. *Soil Dyn. Earthq. Eng.* 173, 108095. doi:10.1016/j.soildyn.2023.108095
- Zhang, J. M. (2000). Reversible and irreversible dilatancy of sand. *Chin. J. Geotechnical Eng.* 22 (1), 12–17.
- Zhang, J. M., and Wang, R. (2024). Large post-liquefaction deformation of sand: mechanisms and modeling considering water absorption in shearing and seismic wave conditions. *Undergr. Space* 18, 3–64. doi:10.1016/j.undsp.2024.03.001
- Zhao, K., Xiong, H., Chen, G. X., Zhuang, H. Y., and Du, X. (2017). Cyclic characterization of wave-induced oscillatory and residual response of liquefiable seabed. *Eng. Geol.* 227 (21), 32–42. doi:10.1016/j.enggeo.2017.01.009
- Zhou, X., Stuedlein, A. W., Chen, Y., and Liu, H. (2021). Cyclic strength of loose anisotropically-consolidated calcareous sand under standing waves and assessment using the unified cyclic stress ratio. *Eng. Geol.* 289, 106171. doi:10.1016/j.enggeo.2021.106171
- Zienkiewicz, O. C., Chang, C. T., and Bettess, P. (1980). Drained, undrained, consolidating and dynamic behavior assumptions in soils. *Géotechnique* 30 (4), 385–395. doi:10.1680/geot.1980.30.4.385